11th World Congress on Computational Mechanics (WCCM XI)
5th European Conference on Computational Mechanics (ECCM V)
6th European Conference on Computational Fluid Dynamics (ECFD VI)
E. Oñate, J. Oliver and A. Huerta (Eds)

INVESTIGATION OF INTERSONIC FRACTURE IN HIGLY CURVED COMPOSITE LAMINATES UNDER QUASI-STATIC LOADING

GOZLUKLU B[*†], UYAR I[†] AND COKER D[†‡]

[*] Helicopter Group
Turkish Aerospace Industries (TAI)
Fethiye Mahallesi, Havacılık Bulvarı, 06980, Kazan, Ankara, Turkey
e-mail: burak.gozluklu@gmail.com, www.tai.com.tr

[†] Department of Aerospace Engineering
Middle East Technical University (METU)
Dumlupınar Bulvarı, 06800 Çankaya, Ankara, Turkey
e-mail: imrenuyar@gmail.com, www.metu.edu.tr

[‡] METU Center for Wind Energy
Middle East Technical University (METU)
Dumlupınar Bulvarı, 06800 Çankaya, Ankara, Turkey
e-mail: coker@metu.edu.tr, ruzgem.metu.edu.tr

Key Words: *Intersonic fracture, delamination, cohesive zone method, composite materials.*

Abstract. In wind energy and aerospace industries, new advances in composite manufacturing technology enable to produce primary load carrying elements as composite materials in wide variety of shapes large such as an L-shape. However, due to the geometry, Interlaminar Normal Stresses (ILNS) are induced once a moderately thick laminate takes highly curved shape. In the curved part of the L-shaped structure, the development of ILNS promotes mode-I type of delamination propagation which is the weakest fracture mode. This is a problem that has recently risen to the forefront in in-service new composite civil aircrafts. This study focuses on experimental and computational investigation of dynamic delamination in a 12-layered woven L-shaped CFRP laminates subjected to quasi-static shear loading. Delamination initiation and propagation processes were captured with a million fps high speed camera. A single delamination is found to initiate in the curved region at the 5th interface during a single drop in the load. The delamination is then observed to propagate at intersonic speed of 2200m/s. The experiments are simulated using cohesive elements by implementing bilinear cohesive model into ABAQUS/Explicit. The experiments and computations are found to be in good agreement, at the macroscale in terms of load-displacement behavior and the failure load, and at the mesoscale in terms of the location of delamination nucleation and delamination crack tip speeds. Shear Mach waves emanating from the crack tips are also observed in the simulations during intersonic crack propagation.

1 INTRODUCTION

Composite materials are preferred for both wind turbine and aerospace industries due to their high stiffness and low weight. In wind turbine blades, CFRP stay in a critical position, since it contributes well to the light-weight structures. As manufacturing technology further develops, composite structures have started to be used in different geometries and configurations. However, once the composite structures take complex shapes in the third dimension, the "interlaminar tension stresses" not used to be applied by the industry becomes apparent. Those tension stresses yield delamination; the separation of the lamina. One of the most typical example for delamination due to interlaminar tension stress problem is the L-section composite elements in box structures. By investigating and studying the phenomenon, without adding support structures or material, lightweight L-section can be designed.

When external loads on a main spar of turbine blades is investigated, the loading in a typical L-shaped beams can be reduced to three simple loading cases namely, axial load which is parallel to the arm (P), shear load which is perpendicular to the arm (V), and the moment (M). These external loads cause delamination in the composite laminates in the curved region because of the low through-the-thickness strengths of composites. This paper contains experimental analyses on the dominating fracture mode in L-shaped composite beams called delamination.

Delamination failure in L-shaped composite laminates under perpendicular loading to the arm was investigated in the 1990s by Martin et. al.[1] , [2] who determined numerically the location of highest radial stress in curved region where delamination is assumed to initiate. They showed that delamination propagates in to the arms of the laminate predominantly in opening mode using energy release rate analysis. In their experimental analysis, delamination growth was found to be unstable but the growth of delamination was not captured. In the 2000s, Wimmer et. al. [3] studied the same problem. Their computational models using VCCT showed unstable crack growth for the case without any initial crack and a stable crack growth for a 3-mm pre-crack. In their experimental analysis, they showed the instantaneous load drop in load displacement curve occurred during crack propagation. Feih and Shercliff (2005) [4] also investigated the failure of L-shaped composite laminates positioned between a composite base and vertical rib for perpendicular to the arm loading case. The finite element model is carried out in ABAQUS with UMAT subroutines combined with Hashin's failure criteria for matrix and fiber cracking and with Tong-Norris delamination onset criterion. In numerical results, they showed the failure sequence and failure types with locations and validated by strain gage results in experiments. Gozluklu and Coker [5] carried out explicit finite element analysis with cohesive elements to model delamination in composite L-beams subjected to parallel loading instead of perpendicular loading. In their simulations, they observed dynamic crack growth and the crack tip speed reaching the shear wave speed of the laminate.

2 EXPERIMENTAL METHOD AND MATERIAL

2.1 Material and Specimen

The cross-section of the L-shaped composite laminates used in this study is shown in Fig. 1 (a). The dimensions of the L-shaped composite specimen and the coordinate axis are shown in Fig. 1(a). The lengths of the lower and upper arms are 90 mm and 150 mm, respectively. The inner radius at the corner is 10 mm and the width is 30 mm.

The specimen is made of 12 layers of HexPly® AS4/8552-5HS plain weave fabric plies with a lay-up of $[0/90]_{6s}$. The specimens were manufactured by hand lay-up technique where the pre-pregs with a cured thickness of 0.28 mm were laid up on a right angled male tool. After the curing, thickness of the laminate is measured to be uniformly 3.36 mm. The longitudinal and transverse moduli of the composite laminate are 55.7 GPa and 8.5 GPa, respectively [6]. The Poisson's ratio (ν_{12}) of the laminate is 0.05 [6]. In order to obtain micrographs, the specimens were cut through plane A and plane B in Fig. 1a using a diamond saw cutter and were stabilized in an epoxy mount for microscopic inspection. Optical micrographs show the cross sectional views of the plane weave fabric in planes A and B and after the failure in plane-B in Fig. 1b-d, respectively. The distribution of the 0 degree fibers and 90 degree fibers in the woven plies are shown in Figure 1b and Figure1c. In addition, the post-failure micrographs show that cracks are moving in between the plies but the path is not straight. The specimen is assumed to be transversely isotropic considering the fiber architecture of the plies. By using the transversely isotropic assumption, the shear wave speed and Rayleigh wave speed calculations were conducted by following the steps described in [7]. After calculating the laminate properties for both lay-ups, the stiffness matrices are obtained. The relations between wave speeds and stiffness components as follow [7],

$$c_s = \left(\frac{c_{66}}{\rho}\right)^{1/2} \tag{1}$$

$$\left(\frac{c'_{11}c'_{22}-c'^2_{12}}{c'_{22}c'_{66}} - \frac{\rho v^2}{c'_{66}}\right)\left[\frac{c'_{22}}{c'_{11}}\left(1-\frac{\rho v^2}{c'_{66}}\right)\right]^{1/2} - \frac{\rho v^2}{c'_{66}}\left(1-\frac{\rho v^2}{c'_{11}}\right)^{\frac{1}{2}} = 0 \tag{2}$$

In (1), C_s (1636 m/s) the shear wave speed and ρ is density. For the Rayleigh wave speed calculation, the same steps in [7] were followed. The real root of (2) gives the Rayleigh wave speed as 1572 m/s. In experiments, seven different specimens were used and three of them were reported here.

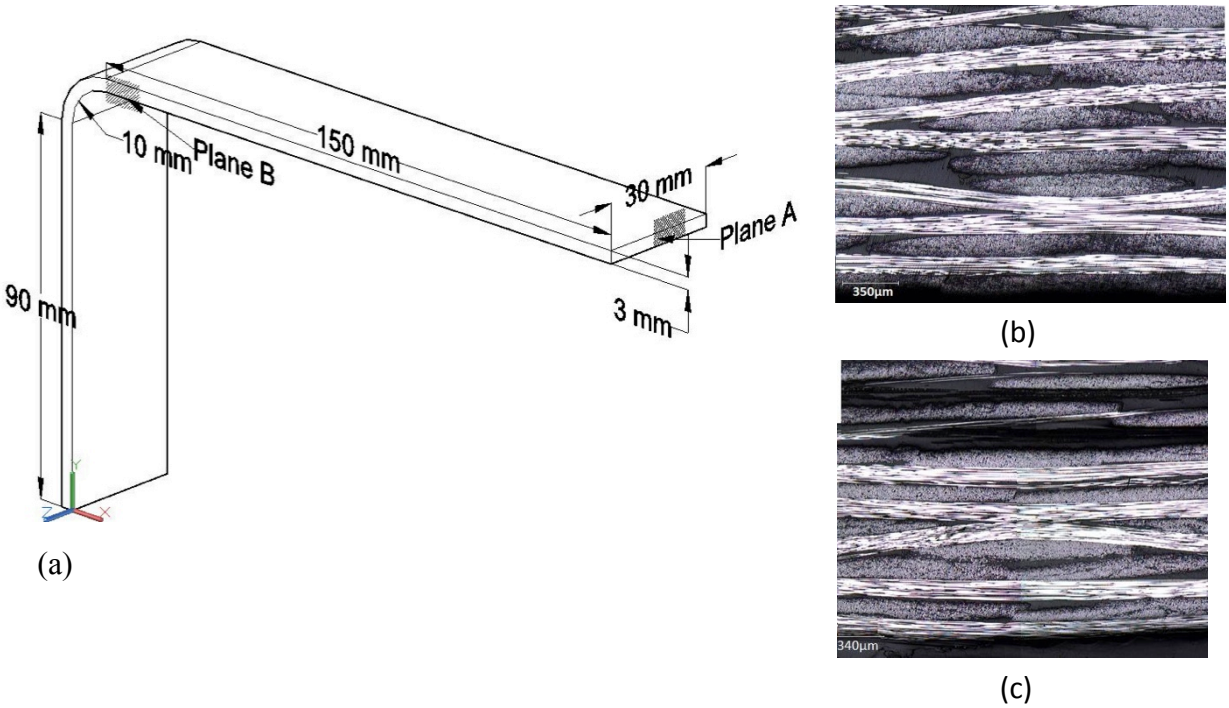

Figure 1: (a) Specimen Geometry (b) Optical micrographs on A-plane of composite specimens showing cross sectional distribution of fibers and epoxy matrix for $[0/90]_{6s}$ in (b) Plane A (c) Plane B

2.2 Experimental Setup

The L-shaped composite beam is subjected to quasi-static shear loading perpendicular to the horizontal arm. The schematic of the experimental fixture that illustrates the loading condition for the L-shaped composite is shown in Fig. 2(a) together with a photograph of the system in Fig. 2(b). The vertical arm of the L-shaped specimen is clamped and bolted to the lower fixture. The fixture is mounted on a linear motion bearing system which is free to move along the x-axis. The sliding part of the fixture gives a smooth precision motion along the x-axis in order to avoid any reaction force along the x-axis to the upper arm [1].The horizontal arm of the specimen is bolted to a pivot pin bearing system in order to fix the arm with respect to the corner of the specimen which is free to rotate around the z-axis. The load-displacement data during the experiment is recorded and an ultra-high speed camera system is used to capture the images of the delamination initiation and propagation. The experimental setup showing the fixture, loading and high speed camera system is shown in Fig. 3.

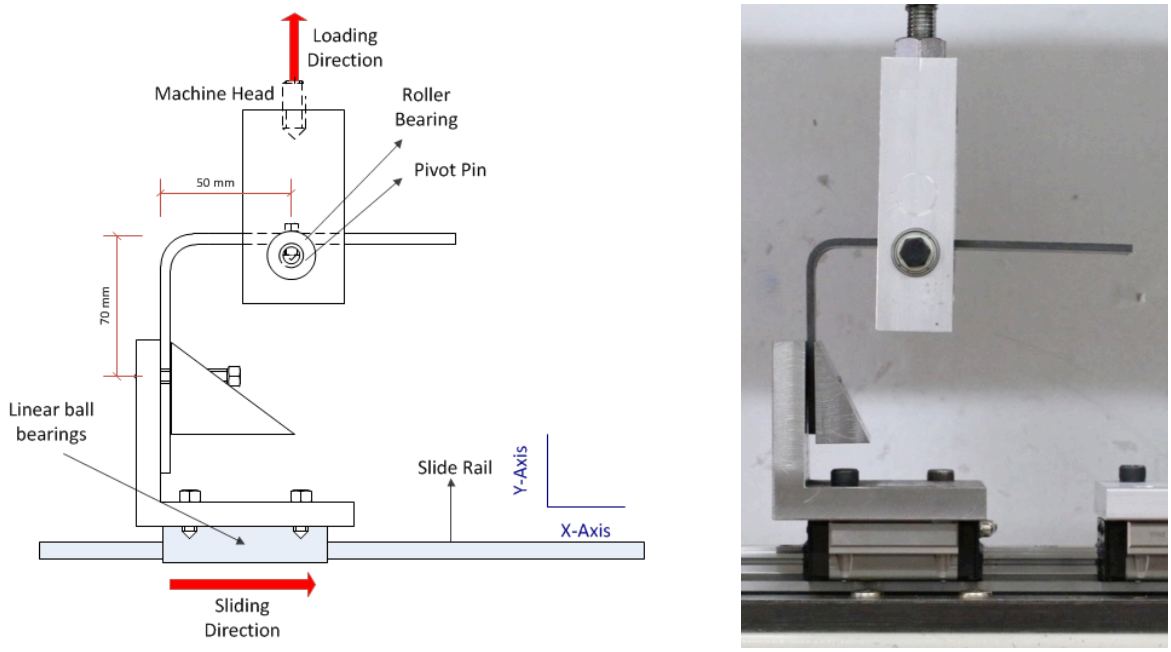

(a) (b)

Figure 2: (a) Schematic of loading fixture for perpendicular loading of the arm; (b) Photo of the fixture and specimen before the experiment

A Shimadzu Autograph AGS-J series with 10 kN capability screw-driven displacement controlled tensile-compression testing machine was used. All tests were conducted at a cross-head speed of 3 mm/min for quasi-static loading. Photron FASTCAM SA-5 high-speed camera system which records the images with framing rates of 7500 fps at full resolution of 1 MP and at 1,000,000 fps at reduced resolution were used. Since the delamination process had been expected to occur at least in the Rayleigh wave speed, the frame rates of 372,000 and 500,000 fps were chosen. A field of view of 17.5 mm x 15.7 mm is recorded using a 50 mm lens with 12.5 mm extension tubes during the experiment. Aerosol-Art Ral 9010 white color was used to paint the side face of the specimen to create a contrast for better visualization of the delamination. The images are recorded continuously about 4-5 seconds (2,000,000 frames at 120x64 pixels) that is saved when the record button is triggered manually at the first crackling sound. The time interval between two pictures is either 2.7 µs or 1.9 µs, where the complete delamination process lasts less than 20 µs in the camera records. The focused area can be captured by 64x120 pixels at the high frame rates. The curved part and the left arm of the specimen were separately focused and recorded with two different high speed cameras for improving the image quality.

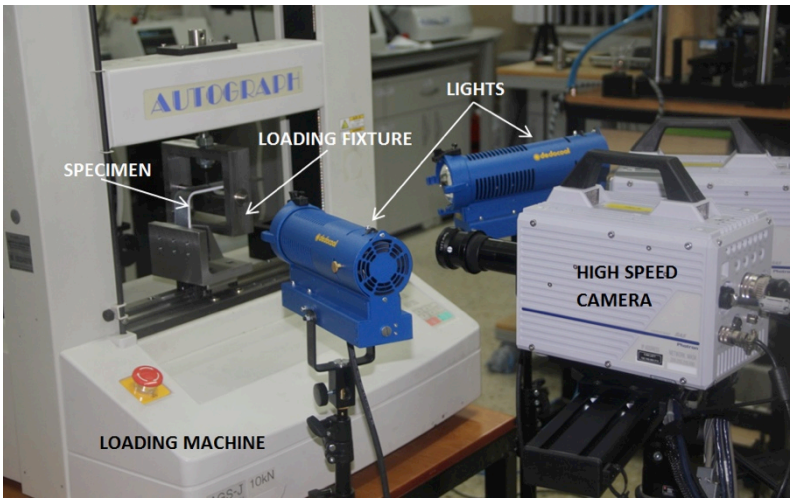

Figure 3: Experimental setup showing the loading fixture, specimen, lighting sources and the Photron SA5 high speed camera.

3 NUMERICAL METHOD

3.1 Cohesive Zone Method

The cohesive zone model (CZM) used in this study is Bilinear CZM that has been proposed by Mi et al. [8].The constitutive law of the CZM is based on surface tractions (T) and relative displacements in mode-I (δ_I), mode-II (δ_{II}) and mixed mode (δ). The constitutive law shows a triangular profile formed by initiation and propagation criteria as shown in Fig 4. The initiation criterion is taken from Chang and Springer [9] that provides a quadratic function based on pure-mode maximum tractions. On the other hand, the propagation criterion is Benzeggagh and Kenane [10] criterion which is based on curve fitting of mixed-mode fracture experimental results. The derivation can be found in Camanho and Davila [11];hence, it is not provided here. The model has been implemented into ABAQUS/Explicit via user-subroutine. The interface element uses Newton-Cotes integration scheme as suggested by Schellekens and de Borst [12].

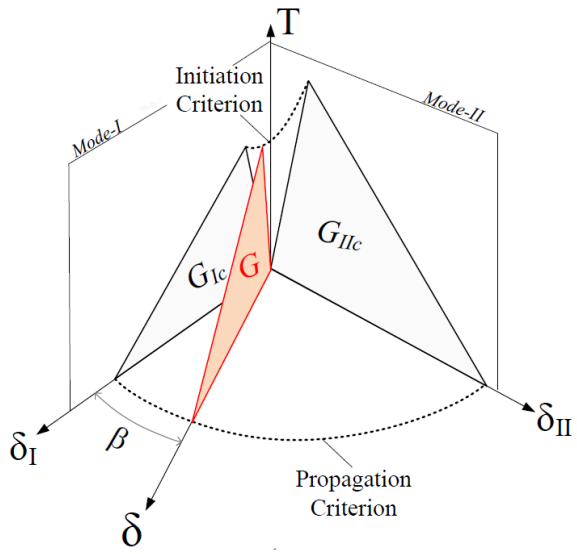

Figure 4: Mixed-mode constitutive law of Bilinear CZM.

3.2 Finite Element Model

The mesh of the L-shaped composite laminate is shown in Fig 5. The length of the arms is 40 mm that represent the region free to deform. The morphology of the mesh is uniform. The width of the elements is 125 µm and the high of the element is 70 µm, which were determined after a rigorous mesh sensitivity study. The tips of the arms are inhibited for delamination propagation since they are clamped in the experimental setup. The tip of the lower arm is clamped, whereas the tip of the right arm is loaded by displacement input with a smooth profile. The interface elements are located at all interfaces. The type of the body elements is made of "CPE4R" elements which is quadrilateral plane strain element with single integration point at the centroid [13]. The total degrees of freedom are 141,120. The stable time increment, Δt, is calculated by ABAQUS as 9.212x10-9 s. Solution duration of a single simulation takes 27 hours and 15 minutes by a 64-bit Intel Core i7-2620M CPU 2.70 GHz with 8 GB RAM computer.

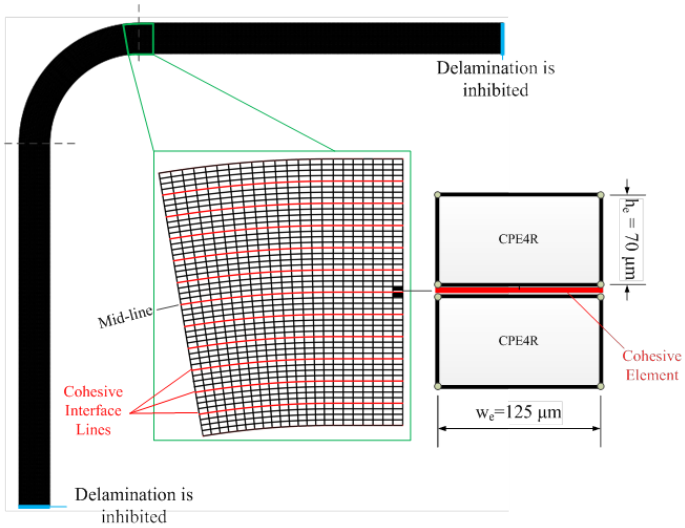

Figure 5: Mesh characteristics of the L-shaped composite laminate finite element model

4 RESULTS

In the simulations and the experiments, the delamination initiated at the 5th interface, the interface between the plies 5 and 6 at the curved region. The load-displacement curve of the experimental specimen F1 and F2 are shown in Fig 6. All delamination takes place between the load levels of A and B as shown in Fig. 6. The failure load and the displacement values are found to be 753 N at U = 19.5 mm for experiment-F1 (F1(Exp.)), 735N at U = 18.7 mm for experiment-F2 (F1(Exp.)) and 762 N at U = 19.4 mm for the simulation (BL) corresponding to point A. The load drop continues around 150N to 200 N for the experiments and simulations when the delamination propagation ends which corresponds to point B.

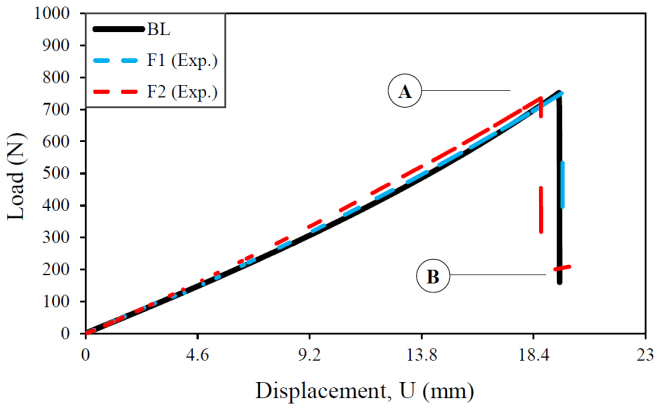

Figure 6: Load-displacement curves for the experiments F1, F2 and the simulation of BL CZM.

Prior to the delamination, the maximum stress of 40 MPa is attained at the opening stress (σ_{33}) as shown in Fig. 7 top. The shear stresses are higher in the arms where the opening stresses are compressive. The longitudinal stresses direct that the beam is under bending. The pictures of stresses indicated that the delamination initiates at the point of maximum opening stress at the curved region under mode-I condition. Afterwards, it propagates along the arms at the 5th interface until reaching the ends of the arms under mode-II dominated loading (Fig. 7-bottom).

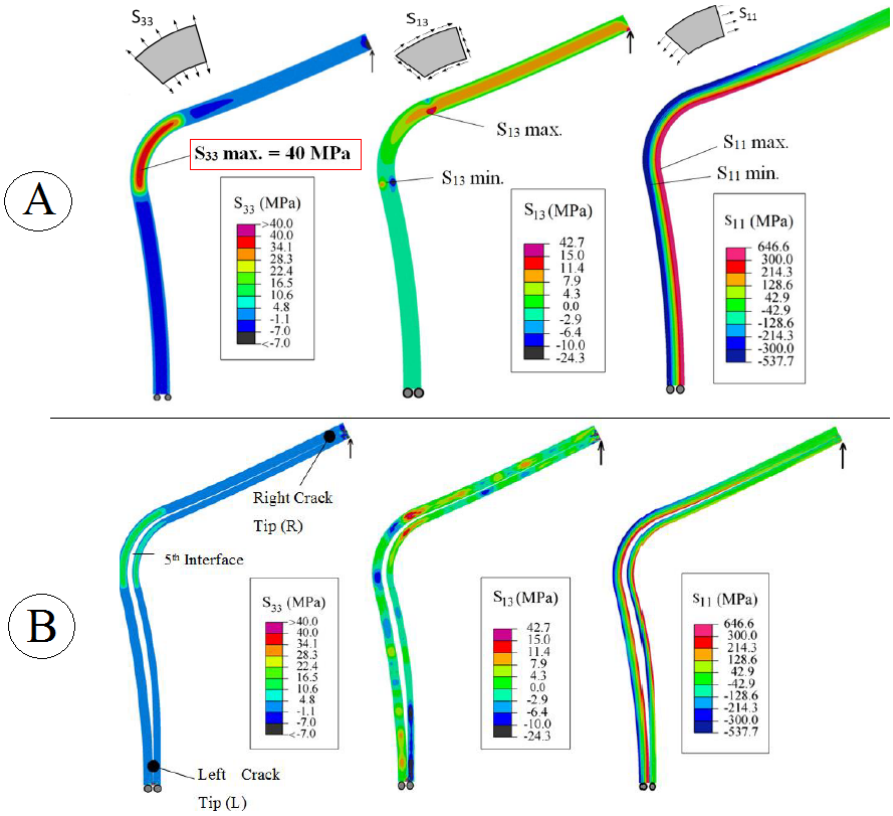

Figure 7: Opening (σ_{33}), shear (σ_{13}), and longitudinal stresses (σ_{11}) for the points A and B.

Delamination initiated at the 5th interface with the angular location of 13° counterclockwise from the centerline as shown in Fig 8-top. The numerical prediction of initiation point is close to the experimental value of 12° at the 5th interface Fig 8-bottom. Delamination continues to propagate to both sides in agreement with experimental results (Fig 8).

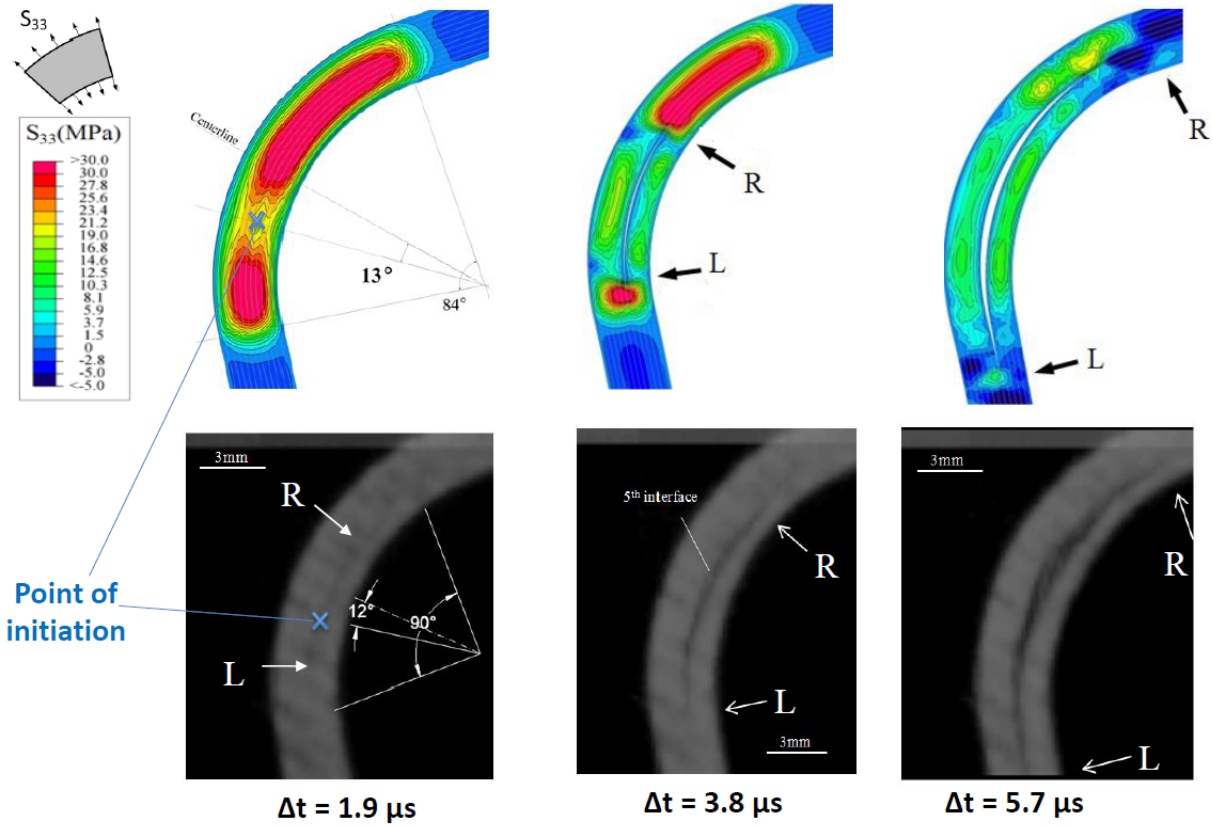

Figure 8: Initiation and propagation of delamination in the curved region obtained from numerical analysis (top) and the high speed camera pictures from the experiment (bottom).

The crack tip speed as a function of time curves found by simulations (BL) and experimental results (F1,F2) for left and right crack tips are shown in Fig 9a and Fig 9b, respectively. It can be seen that the left crack tip propagates at sub-Rayleigh wave speed (C_R) for 7 µs after it accelerated to intersonic speeds ($V>C_s$) for about 9 µs. Delamination propagation continues around 3500 m/s sustainably in the simulations. The experimental results are in agreement with the sub-Rayleigh propagation regime for the left crack tip. On the other hand, the right crack tip speed behaves like the left crack tip except that it cannot sustain its speed at 3500 m/s after when it starts to decelerate. The experimental evidence now supports intersonic crack propagation for the right crack tip. The experimental and numerical results are in good agreement for the crack tip speeds. In the simulations, shear Mach waves are observed in the opening stress contours (σ_{33}) during the intersonic crack propagation. Figure 10 shows motion of the crack tip where the shear Mach waves and the following reflecting waves are observed.

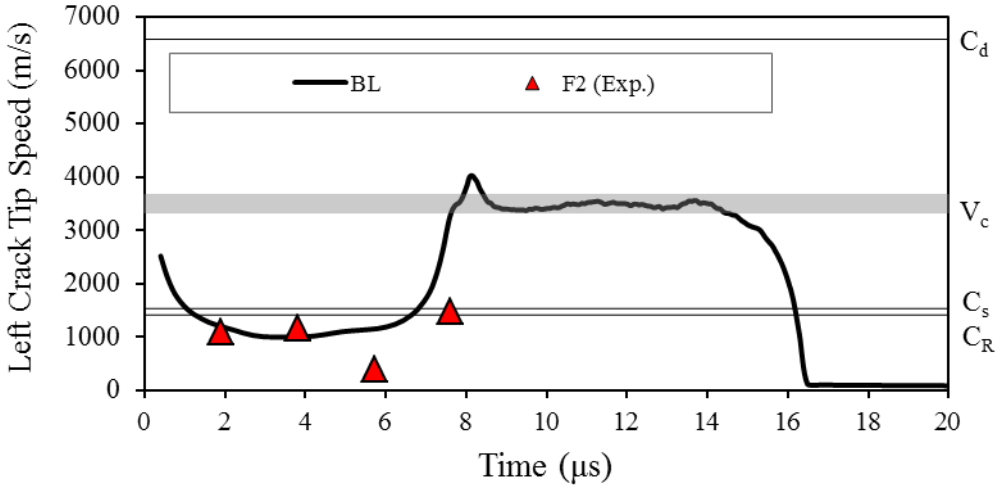

(a)

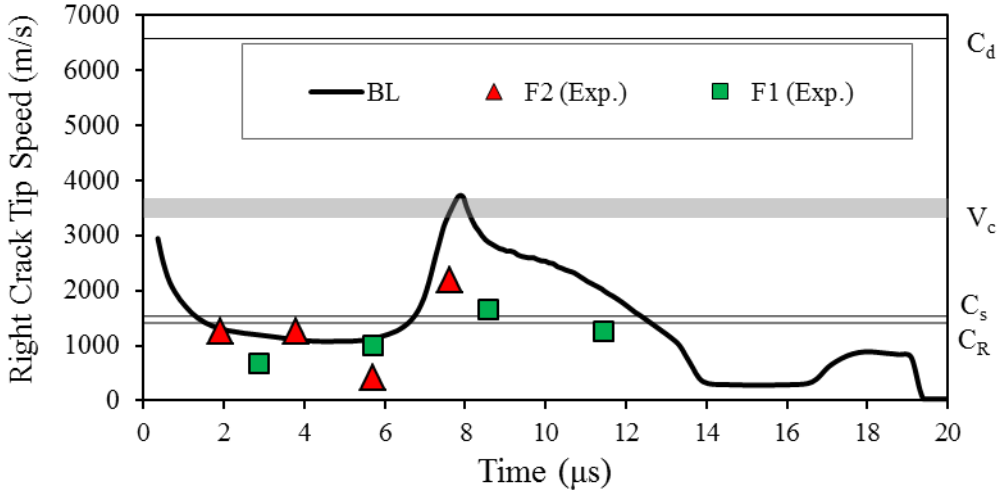

(b)

Figure 9: Crack tip speed as a function of time obtained by simulations (BL) and experimental results (F1,F2) for (a) left and (b) right crack tips.

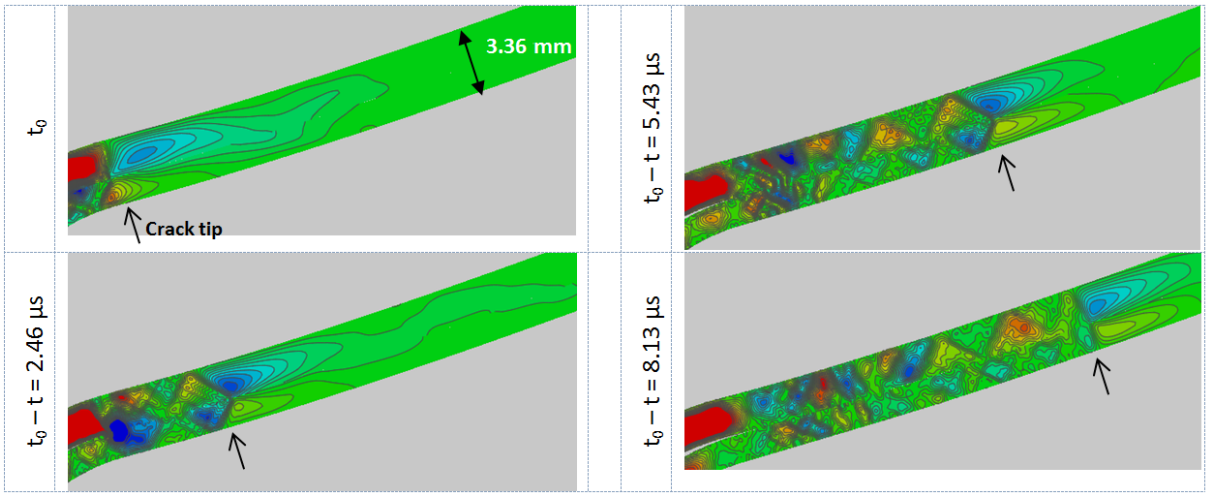

Figure 10: Propagation of right crack tip in the horizontal arm showing shear Mach waves in the opening stress contours.

5. CONCLUSIONS

Dynamic delamination in a woven fabric L-shaped composite laminate under quasistatic loading was studied experimentally using an ultra-high-speed camera and numerically using finite element analysis with a cohesive zone model. Delamination initiation and propagation process was captured and was compared with the numerical results.
The following conclusions can be drawn;

- The experiments and computations agree quite well, at the macroscale in terms of load-displacement curve and the failure load, and at the mesoscale in terms of location of delamination nucleation and delamination crack tip speeds.
- Intersonic delamination is observed in the L-shaped composite laminates under quasi-static loading. Shear Mach wave fronts are captured during the intersonic crack propagation.

To the best of author's knowledge, it is the first time that a intersonic delamination is observed both experimentally and numerically under quasi-static loading which is generally a subject of Geophysics as they are observed in earthquakes such as in the Izmit, Turkey earthquake in 1999 [14].

REFERENCES

[1] Martin R.H., Jackson W.C., Damage prediction in cross-plied curved composite laminates, NASA Technical Memorandum 104089, USAAVSCOM Technical Report 91-B-009; 1991.
[2] Martin R.H., Delamination failure in a unidirectional curved composite laminate, Compos Mater Test; 10:365–83, Des 1992.

[3] Wimmer G., Kitzmüller W., Pinter G., Wettermann T., Pettermann H.E., Computational and experimental investigation of delamination in L-shaped laminated composite components, Eng Fract Mech;76:2810–20, 2009.
[4] Feih S., Shercliff H.R., Composite failu11re prediction of single-L joint structures under bending, Composites Part A 36 (2005) 381-395
[5] Gozluklu, B., Coker, D., "Modeling of the dynamic delamination of L-shaped unidirectional laminated composites," Composite Structures, 94, 1430-1442, 2012.
[6] AS4/8552 Product Data Retrieved from: http://www.hexcel.com/Resources/DataSheets/Prepreg-Data-Sheets/8552_eu.pdf
[7] Coker D., Rosakis A. J.,"Experimental observations of intersonic crack growth in asymmetrically loaded unidirectional composite plates", Philosophical Magazine A, vol. 81, No. 3, 571-595, 2001.
[8] Mi Y, Crisfield MA, Davies GAO, Hellweg HB. "Progressive Delamination Using Interface Elements". Journal of Composite Materials (1998) 32:1246.
[9] Chang F and Springer GS. The strength of fiber reinforced composite bends. Journal of composite materials 1986; 20:30-45.
[10] Benzeggagh ML, Kenane M. Measurement of Mixed-Mode Delamination Fracture Toughness of Unidirectional Glass/Epoxy Composites with Mixed-Mode Bending Apparatus. Composites Science and Technology 1996;56:439–449.
[11] Camanho PP, Davila C. Mixed-Mode Decohesion Finite Elements for the Simulation of Delamination in Composite Materials, NASA/TP-2007-214869, 2002.
[12] Schellekens J, de Borst R. On the Numerical Integration of Interface Elements. International Journal for Numerical Methods in Engineering 1993;36:43-66.
[13] ABAQUS User Manual. Pawtucket (RI); Hibbitt, Karlsson& Sorensen Inc.; 2009.
[14] Bouchon M, Bouin M-P, Karabulut H, Toksöz MN, Dietrich M and Rosakis AJ. How fast is Rupture during an Earthquake? New insights from the 1999 Turkey Earthquakes. Geophysical Research Letters 2001;28(14):2723-2726.